Electronic Supplementary Material (ESI) for Nanoscale.

Supplementary Information

3D $Ti_3C_2T_x$ Aerogel with Enhanced Surface Area for High Performance Supercapacitors

Xinyu Wang,[‡,a] Qishan Fu,[‡,a] Jing Wen,[a] Xinzhi Ma,[a] Chuncheng Zhu,[a] Xitian Zhang[*,a] and Dianpeng Qi,[*,b]

[a] Key Laboratory for Photonic and Electronic Bandgap Materials, Ministry of Education, School of Physics and Electronic Engineering, Harbin Normal University, Harbin 150025, P. R. China.

[b] School of Chemistry and Chemical Engineering, Harbin Institute of Technology, Harbin, 150001, China.

‡ These authors contributed equally to this work.

* Corresponding author. Email address: xtzhangzhang@hotmail.com (X. T. Zhang) and dpqi@ntu.edu.sg (D. P. Qi).

Table S1. Fitting results of XPS peaks for Ti_3C_2.

Region	BE (eV)	Assigned to	Substance	Reference
Ti $2p_{3/2}$ ($2p_{1/2}$)	455.3 (461.5)	Ti-C	Ti_3C_2	[1,2]
	456.3 (461.6)	Ti-N	TiN_x	[3,4]
	455.8 (462.4)	Ti-O	TiO_x ($1.5<x<2$)	[5]
	456.6 (463.2)	Ti-O	TiO_x ($1.5<x<2$)	[5]
	459 (464.4)	Ti-O	TiO_2	[1,2]
O 1s	530.2	O-Ti	TiO_2	[1]
	531.1	O-Ti	TiO_x,	[5]
		-O	Ti_3C_2-O_x	[5]
	532.2	O-H	Ti_3C_2-$(OH)_x$	[6]
	532.3	O-N		[7]
	532.5	C-O	C	[1]
	533.4	O-C=O		[8]
	533.5	H-O-H	H_2O	[6]
N 1s	397.8	N-Ti	Ti_3C_2-N	[9]
	399.9	-NH	Ti_3C_2-NH	[1]
	401.0	$-NH_2$	Ti_3C_2-NH_2	[1]
	402.4	N-O		[1]

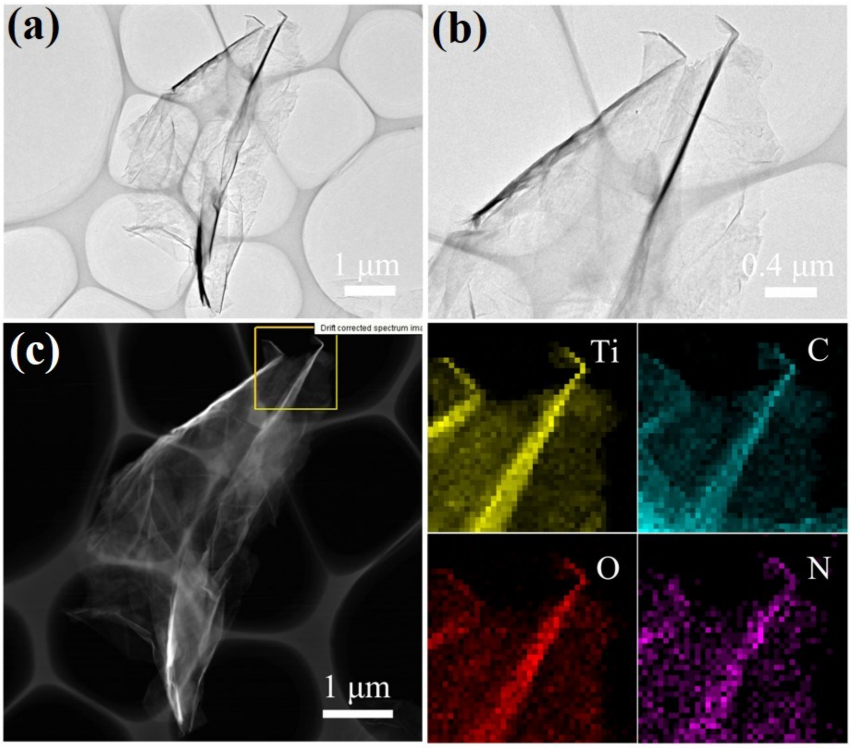

Fig. S1 (a-b) TEM images of the $Ti_3C_2T_x$ aerogel with different magnifications. (c) Elemental mapping images of $Ti_3C_2T_x$ aerogel.

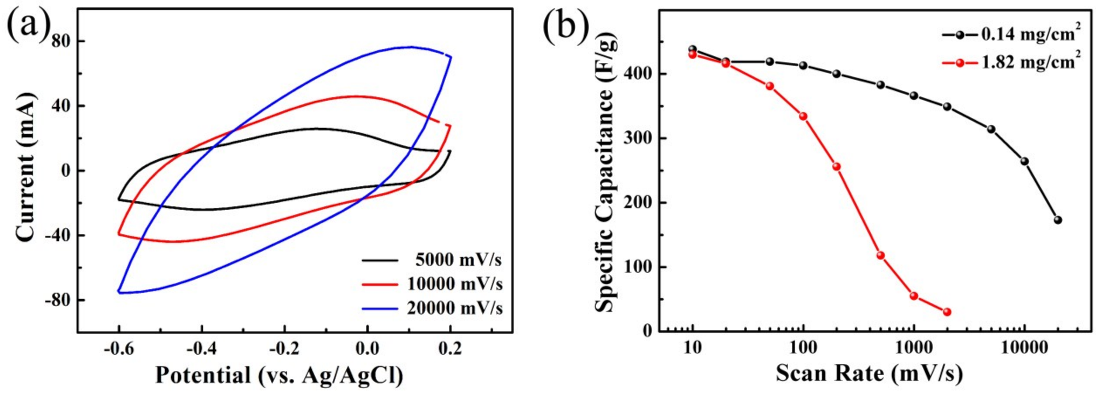

Fig. S2 (a) CV curves of the $Ti_3C_2T_x$ aerogel materials at higher scan rates to 20,000 mV/s. (b) Comparison of mass loading of $Ti_3C_2T_x$ aerogel at different scan rates.

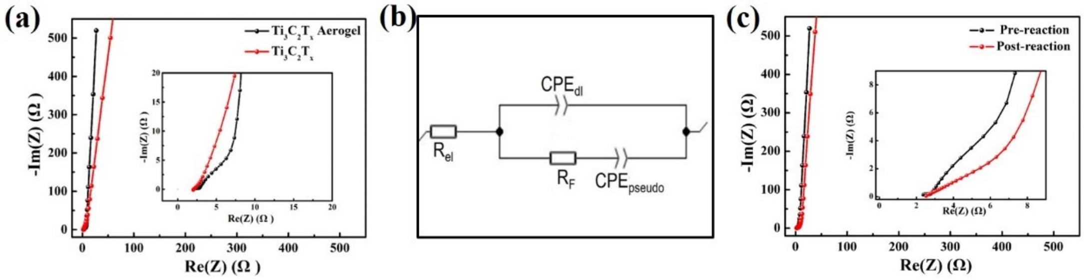

Fig. S3 (a) EIS spectra of the $Ti_3C_2T_x$ aerogel and pure $Ti_3C_2T_x$ electrode materials. Inset shows a magnified high-frequency region. (b) Equivalent circuit. (c) EIS spectrum before and after cycle measurement.

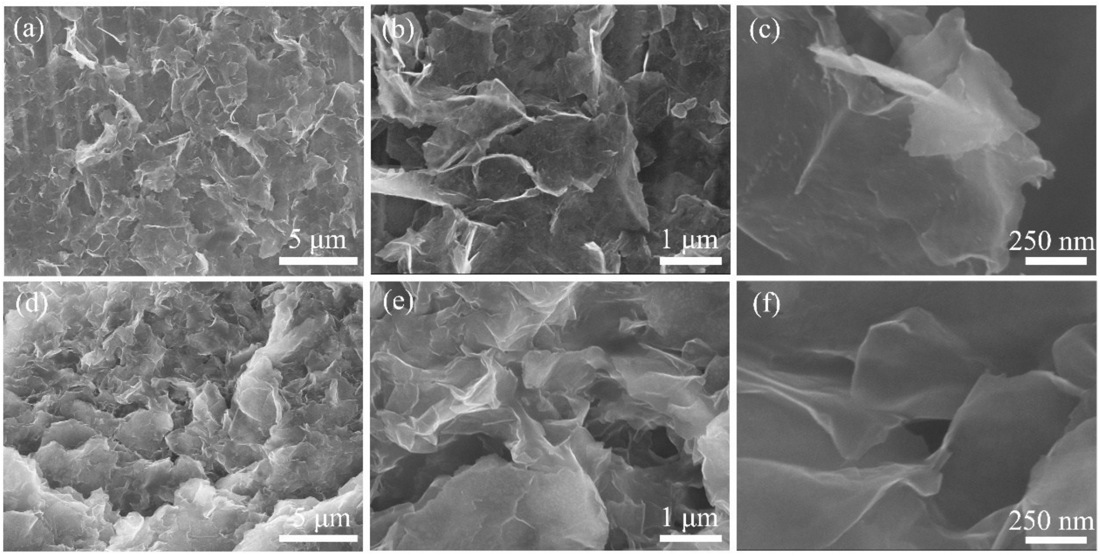

Fig. S4 (a-c) SEM images of the $Ti_3C_2T_x$ aerogel before electrochemical test and (d-f) after electrochemical reaction with different magnifications.

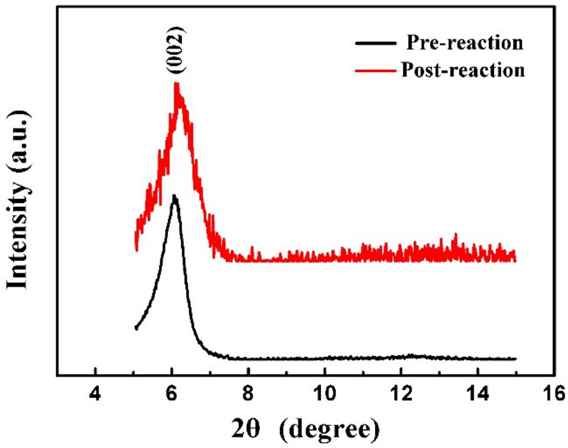

Fig. S5 XRD patterns of the $Ti_3C_2T_x$ aerogel before and after electrochemical reaction.

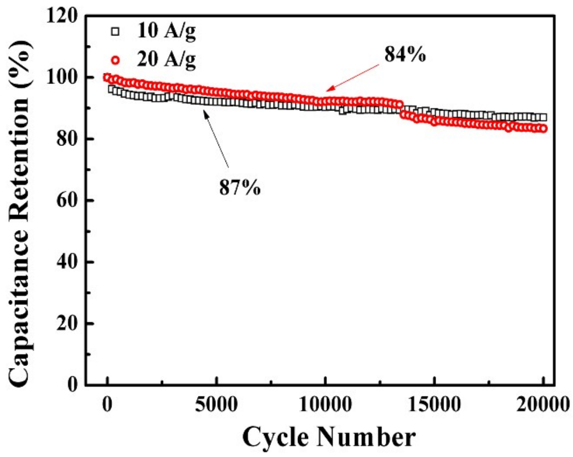

Fig. S6 Cycling performances of pure$Ti_3C_2T_x$ electrode materials at current densities of 10 A/g (black curve) and 20 A/g (red curve).

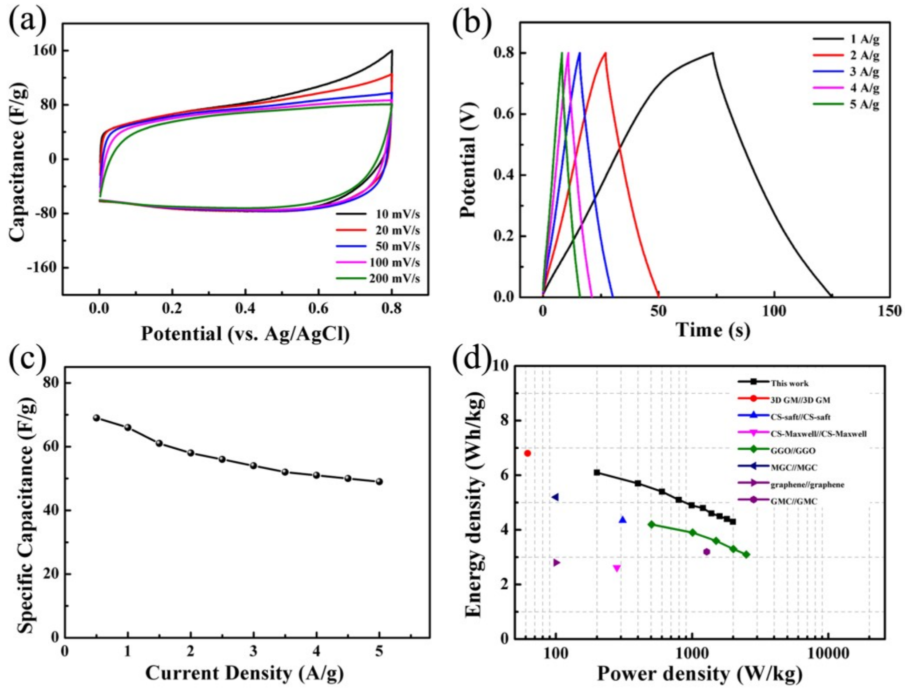

Fig. S7 (a) CV curves at different scan rates of SC. (b) GCD curves at different current densities in the voltage range of 0-0.8 V. (c) Specific capacitance as a function of current density. (d) Ragone plots of the $Ti_3C_2T_x$ aerogel SC. The values reported for other SCs are added for comparison.

A symmetric supercapacitor (SC) is assembled based on $Ti_3C_2T_x$ aerogel electrode. The CV curves of the SC at different scan rate are quasi-rectangular in shape, as shown in Fig. S7a, even at a high scan rate of 200 mV s^{-1}, indicating a high rate capability. And as shown in Fig. S7b, the GCD curves are perfectly linear at different current densities. The specific capacitance calculated from GCD curves are shown in Fig. S7c, and it decreases from 69 to 49 F g^{-1} as the current density increases by 10 times, the corresponding capacitance retention is 71%. Such high rate performance may be ascribed to superior electrical conductivity and porous structure of $Ti_3C_2T_x$ aerogel electrode. Energy density and power density are two important parameters for the SC, and Fig. S7d shows the Ragone plot of our SC calculated from galvanostatic discharge curves. The SC exhibits the higher energy density of 6.1 Wh kg^{-1} and higher power density of 1992 W kg^{-1}. As compared to other SCs reported previously, our $Ti_3C_2T_x$ aerogel SC exhibits a high energy density and power density.

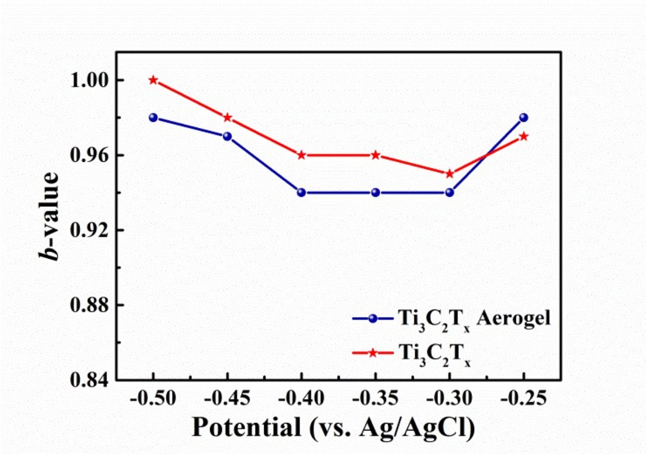

Fig. S8 *b*-values of $Ti_3C_2T_x$ aerogel and pure $Ti_3C_2T_x$ electrode materials at different potentials.

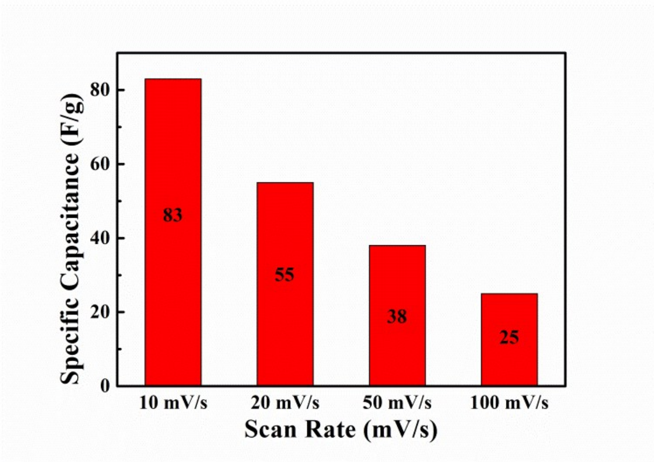

Fig. S9 Specific capacitance from the diffusion-controlled process for the $Ti_3C_2T_x$ aerogel electrode materials at different scan rates.

References

1. T. K. Zhao, J. K. Zhang, Z. Du, Y. H. Liu, G. L. Zhou and J. T. Wang, *Electrochim. Acta*, 2017, **254**, 308-319.
2. J. Halim, K. M. Cook, M. Naguib, P. Eklund, Y. Gogotsi, J. Rosen, M. W. Barsoum, *Appl. Surf. Sci.*, 2016, **362**,406-417.
3. F. Du, H. Tang, L. Pan, T. Zhang, H. Lu, J. Xiong, J. Yang and C. F. Zhang, *Electrochim. Acta*, 2017, **235**, 690-699.
4. Y. F. Zhang, Y. F. Zheng, Y. L. Li, L. X. Wang, Y. J. Bai, Q. Zhao, X. L. Xiong, Y. Cheng, Z. H. Tang, Y. Deng and S. C. Wei, *Plos one*, 2015, **10**, e0130774.
5. Q. S. Fu, J. Wen, N. Zhang, L. L. Wu, M. Y. Zhang, S. Y. Lin, H. Gao and X. T. Zhang, *RSC Adv.*, 2017, **7,** 11998-12005.
6. X. Xu, H. Li, Q. Q. Zhang, H. Hu, Z. B. Zhao, J. H. Li, J. Y. Li, Y. Qiao and Y. Gogotsi, *ACS Nano* 2015, **9**, 3969-3977.
7. H. Binder and D. Sellmann, *Z. Naturforsch*, 1978, **33b**, 173-179.
8. H. R. Byon, B. M. Gallant, S. W. Lee and Y. Shao-Horn, *Adv. Funct. Mater.*, 2013, **23**, 1037–1045.
9. M. Kawamura, Y. Abe, H. Yanagisawa, K. Sasaki, *Thin Solid Films*, 1996, **287**,115-119.
10. Y. H. He, W. J. Chen, X. D. Li, Z. X. Zhang, J. C. Fu, C. H. Zhao and E. Q. Xie, *ACS Nano*, 2013, **7**, 174-182.
11. A. Chu and P. Braatz, *J. Power Sources*, 2002, **112**, 236-246.
12. S. S. Balaji, M. Karnan and M. Sathish, *Int. J. Hydrogen Energ.*, 2018, **43**, 4044-4057.
13. Z S Wu, W Ren, D W Wang, F Li, B Liu and H M Cheng, *ACS Nano*, 2010, **4**, 5835-5842.
14. Y. W. Cheng, S. T. Lu, H. B. Zhang, C. V. Varanasi and J. Liu, *Nano Lett.*, 2012, **12**, 4206-4211.